


A Rapid One-Pot Synthesis of CuO Rice-Like Nanostructure and Its Structural, Optical and Electrochemical Performance

M. PARTHIBAVARMAN ^{1,4}, V. SHARMILA,¹ P. SATHISHKUMAR,²
and SUCHETA ABHAY GAIKWAD³

1.—PG and Research Department of Physics, Chikkaiah Naicker College, Erode, Tamilnadu 638 004, India. 2.—School of Advanced Sciences, VIT University, Vellore, Tamilnadu 632 014, India. 3.—Department of Chemistry, Sir Parshurambhau College, Sadashiv Peth, Pune 411030, India. 4.—e-mail: varmanphysics85@gmail.com

We report the production of high stable rice-like CuO nanostructures synthesized by a facile and one-step hydrothermal method using urea as a fuel agent. The thermogravimetric nature, phase purity, morphology, and structure of rice-like CuO nanostructures have been characterized by thermogravimetric–differential thermal analysis, powder x-ray diffraction (PXRD), field-emission scanning electron microscopy (FESEM), and energy dispersive x-ray spectroscopy. PXRD revealed the formation of monoclinic CuO with an average crystallite size of around 20 nm. FESEM showed a rice-like morphology with an average size of 40–50 and 100–120 nm along the shorter axis and longer axis, respectively. UV-DRS analysis confirmed a considerable blue-shift in the optical band gap ($E_g = 1.45$ eV) owing to a quantum confinement effect. X-ray photoelectron spectroscopy and electron paramagnetic resonance spectra confirmed the presence of copper in Cu^{2+} state. Furthermore, we can use these electrodes for their electrochemical supercapacitive properties, like cyclic voltammetry, galvanostatic charge/discharge and electrochemical impedance spectra. The nano-rice CuO showed an enhanced specific capacitance of 305 F/g at a current density of 1 A/g.

Key words: CuO, rice-like, hydrothermal, optical properties, electrochemical energy storage, pseudocapacitors

INTRODUCTION

Supercapacitor-based energy storage materials are more flexible, smart and lightweight owing to their higher specific power density, extensive charge–discharge, cyclic stability and capacity and fast recharge ability compared to batteries and conventional capacitors. In recent times, transition metal oxides have been of tremendous interest in materials research because of their outstanding optical, electrical, magnetic, and catalytic properties, and widespread applications in practical devices, particularly as promising electrode materials for energy-saving electrochemical capacitors

owing to their numerous oxidation states and higher theoretic specific capacitances than carbon-based nanomaterials.^{1–4} Among various metal oxide-based super-capacitors such as NiO,⁵ CoO,⁶ MnO⁷ and Fe₂O₃,⁸ copper oxides (CuO) have been shown to be promising electrode materials for pseudocapacitor applications due to their remarkable conductivity, higher capacitance, and long-term stability. Moreover, they have low cost of production, good chemical stability and an environmentally friendly nature. Generally, the electrochemical behavior of CuO is very greatly influenced by their significant structure, and their desired morphology with high surface area is essential to enhance the energy and power densities of supercapacitors and pseudocapacitive materials.

Nanostructure CuO with different morphology and dimensions, such as nanotubes,⁹ nanowires,¹⁰

(Received February 24, 2018; accepted June 5, 2018;
published online June 18, 2018)

nanosheets¹¹ and nanoneedles¹² have been synthesized by using several methodologies such as sol-gel, thermal oxidation, electrochemical, hydrothermal, and template using carbon and sonochemical methods. In an attempt to further improve the electrochemical performance; we have prepared a rice-like CuO nanostructure by using a facile hydrothermal method. Among the above methods, the hydrothermal method is very attractive for the production of CuO nanostructures due to its easy manipulation, scalable production, well-defined size, desired morphology, operation simplicity and cost-effectiveness.¹³ However, to the best of our knowledge, a novel and one-step hydrothermal energy-efficient synthesis of rice-like CuO, and scientific studies on its formation mechanism by combining the experimental results with atomic level crystal structure transformations, have not been reported. We report on the thermal, structural, optical and electrochemical behavior of the CuO nanostructure by using a simple and one-step hydrothermal method. Moreover, the possible growth mechanism for the formation of CuO nanostructures is proposed.

EXPERIMENTAL

Materials

Copper nitrate [$\text{Cu}(\text{NO}_3)_2$], purity 99.97%, urea [$\text{CO}(\text{NH}_2)_2$], liquid ammonium hydroxide solution (NH_4OH , purity 99.97%) were used as the precursor solution for the CuO nanostructures. All the chemicals were of analytical grade, purchased from Merck, India, and used without any further purification.

Experimental Details

The CuO nanostructures were prepared by a simple hydrothermal process using urea as the fuel agent. In a typical experimental procedure, 0.1 M $\text{Cu}(\text{NO}_3)_2$ was dissolved in 50 mL distilled water under strong magnetic stirring until completely dissolved. The urea was added to the solution and stirred for 30 min. The ratio of $\text{Cu}(\text{NO}_3)_2$ and urea was 1:2. Then, 25 mL aqueous solution of NH_4OH was added dropwise under strong magnetic stirring until the pH value reached 10. During this reaction, the drop rate must be controlled to achieve chemical homogeneity. Then, the solution was transferred into a Teflon-lined stainless steel autoclave, which was sealed and maintained at different temperatures, such as 100°C, 120°C and 150°C for 24 h. After completing the hydrothermal reaction, the resulting precipitate was thoroughly washed by repeating the procedures of suspending the gel in deionized water and ethanol, then collecting it back by centrifugation to remove Cl^- and NH_4^+ ions, and dried in air in a laboratory hot air oven at 100°C for 10 h. Finally, the light gray colored CuO nanopowder was obtained. The schematic representation for CuO under hydrothermal reaction is shown in Fig. 1. The CuO rice-like structure was achieved from the self-aggregation and decomposition of the precursor $\text{Cu}(\text{NO}_3)_2$ and $\text{CO}(\text{NH}_2)_2$ via a hydrothermal method. The nanoparticles which initially serve as building blocks of many spheres were synthesized at a large scale by a precipitation between $\text{Cu}(\text{NO}_3)_2$ and $\text{CO}(\text{NH}_2)_2$ at room temperature. Under the hydrothermal condition, many CuO rice-like nanocrystals were formed by the decomposition of precursors according to the reaction:

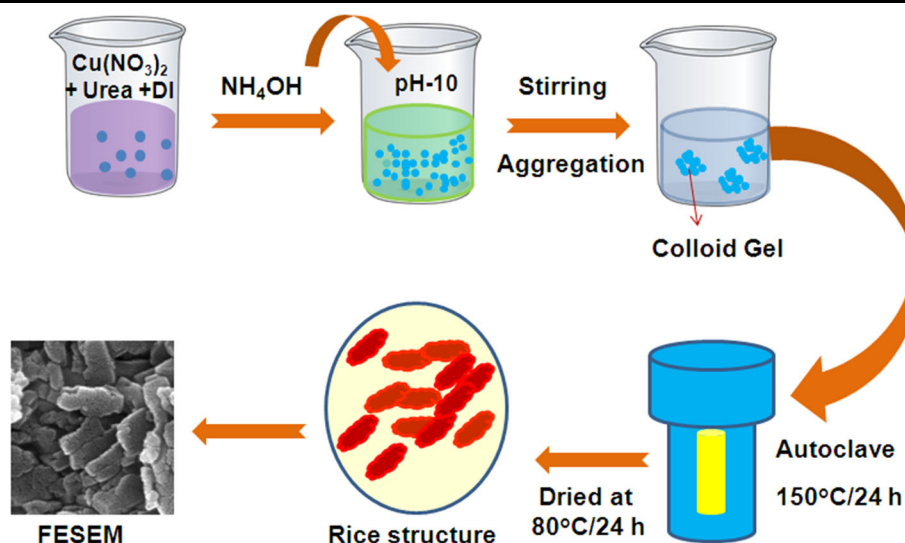
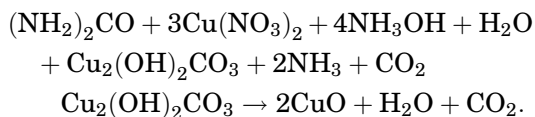


Fig. 1. Schematic representation for rice-like CuO under hydrothermal condition.



During the high-energy hydrothermal reaction, the CuO nanoparticles gradually grow and convert into a CuO nano-rice-like structure.

Characterization

The thermal analysis was performed on a SDT Q600 V8.3 Build 101 thermogravimetric–differential thermal analysis (TG–DTA) system. The heating rate was $10^\circ\text{C min}^{-1}$ in nitrogen flow (40 mL min^{-1}) and the weight of the sample taken in the experiment was around 5 mg. Identification of the crystalline phase and the size of the CuO nanopowder was achieved using powder x-ray diffraction (PXRD) (Bruker diffractometer) using a $\text{CuK}\alpha$ wavelength of 1.5406 \AA and operating at 35 kV and 30 mA. PXRD patterns were recorded in the range 20° – 80° at the scan rate of 0.50 s . Morphology and particle size of the prepared nanoparticles was studied employing a field-emission scanning electron microscope (JEOL-JSM-6390) operating at 15 kV. The elemental analysis of the samples was analyzed through energy dispersive spectroscopy (EDS) (JEOL Model JED–2300). The Raman spectra of the samples were recorded using a BRUKER RFS 27 stand-alone FT-Raman Spectrometer at a resolution of 0.2 cm^{-1} . The optical properties were analyzed by UV–VIS diffusion reflectance spectroscopy using a CARY 5E UV–VIS-NIR spectrophotometer in the wavelength range of 200–1200 nm. Photoluminescence spectra of the samples were recorded using a PerkinElmer LS 55 spectrometer equipped with a He–Cd laser source; the excitation length used was 325 nm. X-ray photoelectron spectroscopy (XPS) was carried out using a Thermo Scientific K-alpha surface analysis instrument.

Electrode Preparation

The electrochemical nature of the as-prepared CuO was investigated with cyclic voltammetry (CV), charge–discharge and impedance spectra analysis by using a software-controlled predictable three-electrode electrochemical cell (CHI 660C electrochemical workstation) consisting of a glassy carbon electrode as the working electrode, Ag/AgCl as the reference electrode, and platinum wire as the counter-electrode. In the preparation of the electrodes, 0.05 g of CuO nanopowder was put into 500 μL of ethanol and then dried at room temperature for 15 min. The working electrode was coated with 0.5 μL of active material dispersed in 5% of 2 μL nafion binder solution. All the electrochemical measurements were performed in a 0.2-M KOH aqueous electrolyte solution at room temperature. The CV measurements were performed at scan rates of 50 mV s^{-1} and 100 mV s^{-1} . A potential

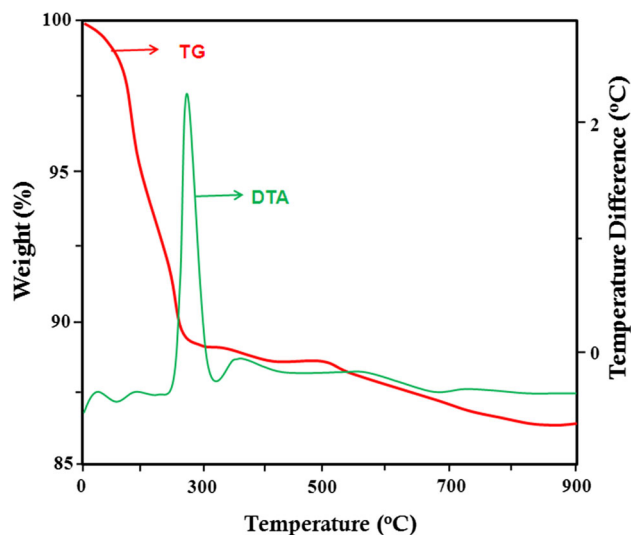


Fig. 2. TG–DTA curve of as-synthesized CuO nanopowders.

window in the range from -0.2 V to 0.8 V was used in all the measurements.

RESULTS AND DISCUSSION

TG–DTA Analysis

The TGA/DTA profile of the as-synthesized CuO is shown in Fig. 2. The TGA curve demonstrates a two-step decomposition of the precursor to form the CuO. The first weight loss below 250°C ($\sim 8\%$) originates from the evaporation of ammonia, water, carbonate ions (the byproduct from urea decomposition) and nitrate ions (from the starting material). The second weight loss (500 – 800°C) is owing to the carbon group compounds and also the loss of oxygen in the CuO nanostructure during the heat treatment.¹⁴ The DTA curve shows an exothermic peak at around 275°C , which may be ascribed to the reaction responsible for the formation of the CuO.¹⁵ This result suggests the formation of rice-like CuO from the copper nitrate precursor solution under the hydrothermal reaction process.

Powder XRD Analysis

In order to confirm the effect of temperature on the crystalline nature and average grain size of the as-synthesized CuO products, PXRD was carried out and the corresponding profile is presented in Fig. 3. It can be clearly seen that all three samples could be indexed to the formation of single-phase CuO crystallized with a monoclinic structure,¹⁶ and the calculated unit cell parameter values, $a = 4.60345 \text{ \AA}$; $b = 3.37129 \text{ \AA}$; $c = 5.11389 \text{ \AA}$; cell volume = $78.0218 \times 10^{-3} \text{ pm}^3$ were in good agreement with the standard values (JCPDS file No. 65-2309).¹⁷ No other impurity phases were detected, such as $\text{Cu}(\text{NO}_3)_2$ or Cu or Cu_2O , which indicates the purity of the samples. Furthermore, the

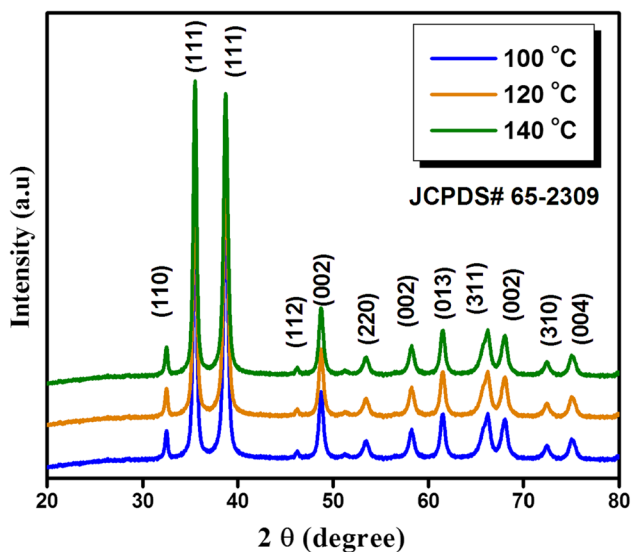


Fig. 3. Powder XRD pattern of CuO with different hydrothermal products.

intensity of all the peaks increases with the increase of reaction temperature from 100°C to 150°C, this result suggesting that the crystallinity of the CuO improved. The increase in grain size was also confirmed by Scherrer's formula,¹⁸ and was found to be 13 nm, 17 nm and 20 nm for CuO with 100°C, 120°C and 150°C hydrothermal-assisted samples, respectively. Hence, the high crystalline nature of CuO with the 150°C-assisted sample was characterized for further studies.

FESEM-EDS Analysis

FESEM is a useful technique to obtain the detailed surface morphology and average particle size of CuO nanostructures. Figure 4a–d shows the FESEM images of the as-synthesized CuO with different magnifications. It can be clearly seen that the as-synthesized CuO shows a 1-D rice-like morphology with the average length in the range of 100–120 nm and width in the range of 40–50 nm. More attractively, individual rice-like-shaped structures are associated to their neighbors leading to the formation of interlaced rice-shaped spheres. FESEM-based EDS analysis confirms that the as-synthesized CuO was mainly composed of Cu and O elements with sharp visible peaks (Fig. 4e), and with a minor contribution from carbon which is present as an impurity of the CuO rice-like structure. The calculated atomic ratio of Cu:O is approximately 55:35, indicating the presence of CuO rather than Cu₂O.

XPS Analysis

In order to further confirm the chemical composition and valance state of the CuO, an XPS survey spectrum was carried out (Fig. 5a), and the

preferred area scans for the individual elements in Cu 2p and O 1s are shown in Fig. 5b and c, respectively. It can be seen that the binding energy of the Cu 2p core level spectrum (Fig. 5b) located at 937.4 eV and 956.7 eV, which is related to the Cu 2p_{3/2} and Cu 2p_{1/2}, respectively. These values are in good agreement with the already reported literature values.¹⁹ The binding energy of the O 1s core level spectrum (Fig. 5c) located at 530.1 eV, which corresponds to O²⁻ ions in the CuO lattice. These results suggest that the chemical valences of Cu at the surface of the CuO nanoparticles are in the +2 state (Cu²⁺).

Raman Spectra Analysis

In general, Raman spectroscopy is a perceptive probe to realize the crystal symmetry, local atomic arrangements and functional group vibrations of materials.²⁰ Here, we analyzed Raman spectra to characterize the structural information of the as-synthesized CuO nano-rice, and the corresponding profile is depicted in Fig. 6, from which it is clearly evident that there are three Raman peaks, at 281 cm⁻¹, 340 cm⁻¹ and 621 cm⁻¹. For the comparison of the CuO bulk single crystal²¹ with the Raman vibrational, all the Raman peaks are red-shifted about 25 cm⁻¹ and broaden with the downshifts, which is appropriate to the quantum size confinement effects of the CuO nano-rice-like structure. The peak at 281 cm⁻¹ can be assigned to the A_g mode, whereas the peaks at 340 cm⁻¹ and 621 cm⁻¹ can be assigned to the B_g modes.²² Thus, the Raman modes again confirm the CuO crystalline with a monoclinic structure.

UV-DRS Spectra Analysis

UV-Vis spectrophotometry is a key tool to identify the energy structure and optical absorption properties of nanosized materials. The quantum size confinement effect demonstrated by the as-synthesized CuO nano-rices can be further confirmed by UV-Vis-DRS analysis, and the corresponding spectra is shown in Fig. 7, from which it can be seen that the broad absorption band edge is found at around 500–800 nm. In order to further confirm the band gap (E_g), we have used the Kubelka–Munk (K–M) model.²³ The K–M model at any wavelength is given by $F(R_\infty) = (1 - R)^2/2R$, where R is the percentage of reflectance. A graph plotted between $[F(R_\infty) h\nu]^2$ versus $h\nu$ and the intercept value is the direct band gap energy,²⁴ and the band gap energy of CuO was found to be 1.45 eV. The experimental band gap energy was somewhat larger than that of the bulk CuO (1.2 eV), which can be attributed to the quantum confinement effect of the rice-like CuO. Similar findings were observed for CuO nanoflakes synthesized by a wet chemical method.²⁵

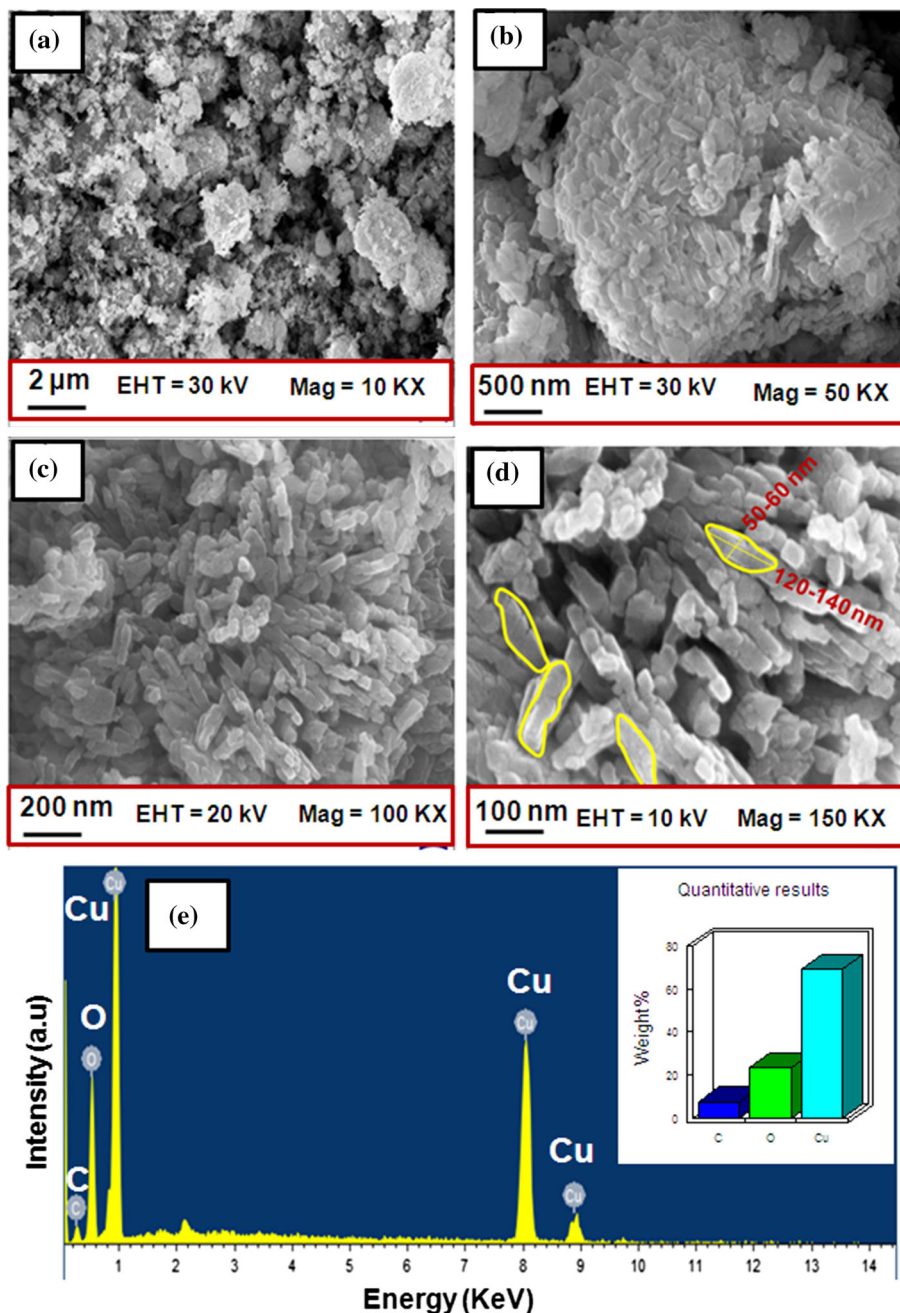


Fig. 4. (a–d) FESEM images of rice-like CuO nanostructures with different magnifications. (e) EDS spectra of CuO.

EPR Analysis

Electron paramagnetic resonance (EPR) is a responsive spectroscopic method to examine the electronic structure and spatial distribution of paramagnetic species on the samples. The local structures of $3d_9$ paramagnetic ions are characterized by means of EPR spectroscopy. Figure 8 presents the room temperature EPR spectra of CuO recorded at room temperature using a Varian E 112, operating at an X-band frequency 8.5–9.5 GHz. Generally, the EPR powder spectrum of copper gives four lines corresponding to the parallel

hyperfine splitting of the copper nucleus ($I = 3/2$), but it gives a single broad EPR signal due to exchange interaction. The parameter 'g' is determined according to the equation $g = h\nu/\mu_B H_r$, where h is Planck's constant, ν is the microwave frequency and μ_B is the Bohr magneton. The g value calculated from this powder spectrum was 2.06, which indicates the copper is in the + 2 state.

FTIR Analysis

Fourier-transform infrared (FTIR) analysis is a technique used to evaluate the vibrational

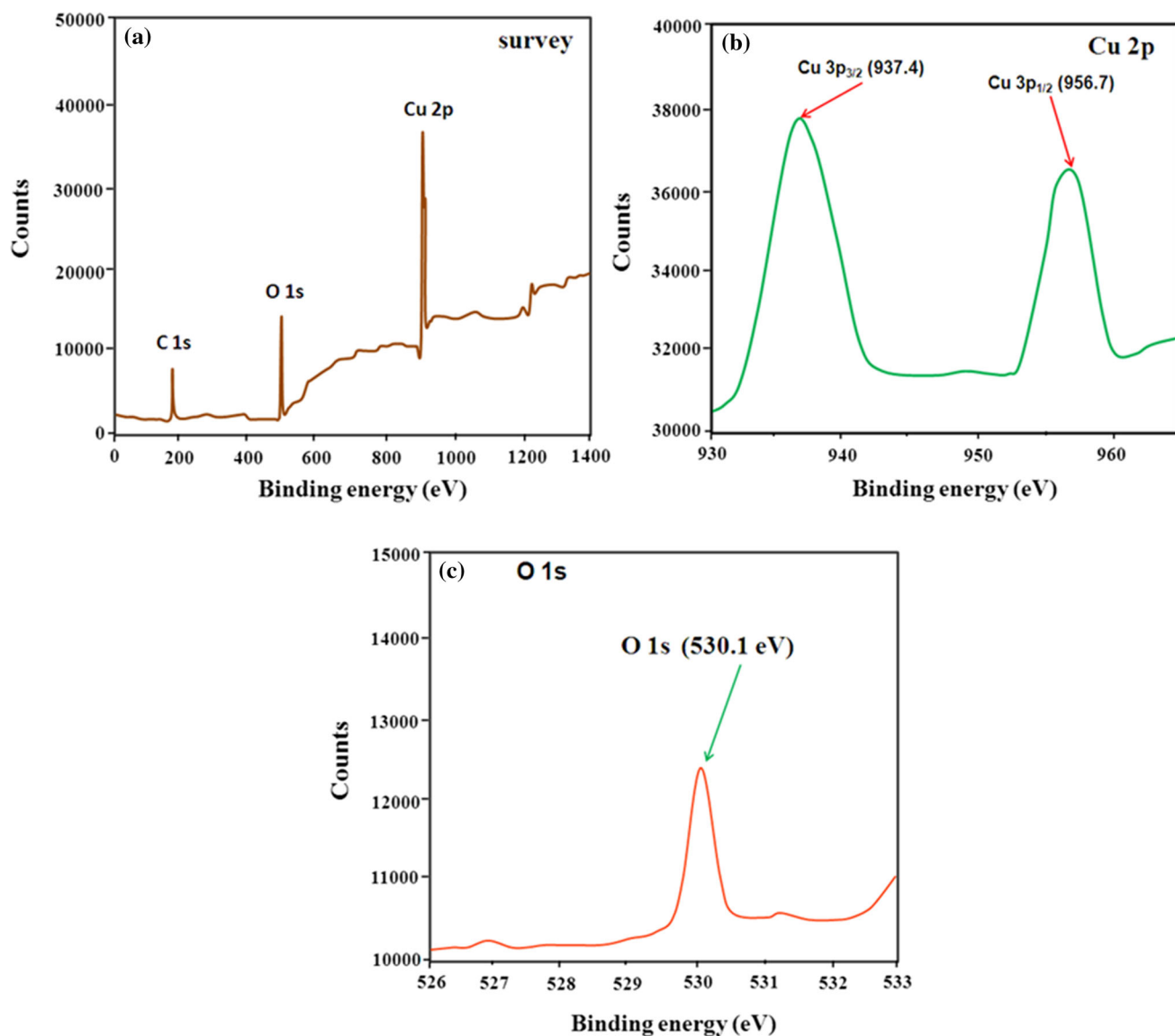


Fig. 5. (a) XPS survey spectrum of CuO, (b) selected area scans for the individual elements in Cu 2p, and (c) O 1s.

frequencies of bonds in the molecule. The FTIR spectrum of CuO is shown in Fig. 9. The broad peaks in the range $3100\text{--}3600\text{ cm}^{-1}$ are attributed to the O–H stretching vibration, which are assigned to a small amount of H_2O existing (during pellet formation) in the nanostructured CuO.²⁶ The carbonate group was identified from the vibration bands at 760 cm^{-1} , 824 cm^{-1} and 1121 cm^{-1} . There are two noticeable absorption peaks at around 562 cm^{-1} and 525 cm^{-1} , which can be assigned to the vibrations of the Cu–O bonds.²⁷ Hence, FTIR analysis revealed that the inorganic component in the sample is a CuO phase with a monoclinic crystal structure. The FTIR results are also in good agreement with the XRD analysis results.

Electrochemical Measurements

CV

The CV technique was performed to study the electrochemical activity of the as-prepared CuO within the potential range of -0.2 V to 0.8 V . CV curves of CuO electrode are shown in Fig. 10a, run at different scan rates ($20\text{--}100\text{ mV/s}$). A pseudocapacitance nature was found for the CuO electrode, which is evident from the quasi-rectangular shape of the CV curves. The anodic and cathodic peaks are shifted to higher and lower potentials due to the increase in the scan rate. In contrast, increasing the scan rate reduces the specific capacitance of all the electrodes. The reduction in the specific capacitance

at higher scan rates is attributed to the diffusion effect of protons within the electrode, and at lower scan rates the reduction takes place due to the existence of inner active sites. These undergo complete redox transitions and tune the specific capacitance efficiency.

Galvanostatic Charge/Discharge

Figure 10b shows the galvanostatic charge/discharge plots of CuO electrode materials for various current densities (1 A/g, 2 A/g, 3 A/g, 4 A/g and 5 A/g). It is found that the specific capacitance value slowly decreases with increase of current density.

The calculated specific capacitances of the CuO electrode were 305 Fg^{-1} , 278 Fg^{-1} , 235 Fg^{-1} , 226 Fg^{-1} and 145 Fg^{-1} at discharge current densities of 1 Ag^{-1} , 2 Ag^{-1} , 3 Ag^{-1} , 4 Ag^{-1} , and 5 Ag^{-1} , respectively. For a better understanding, the graph has been plotted between the specific capacitance and the current density, as shown in Fig. 10c. The calculated specific capacitance values by charge discharge are lower than the values obtained by CV techniques. This is due to inadequate Faradic redox reactions arising from the reduced surface attainment by OH ions in the higher discharge current density conditions. The CV was observed at particular scan rates does not hinder the full surface

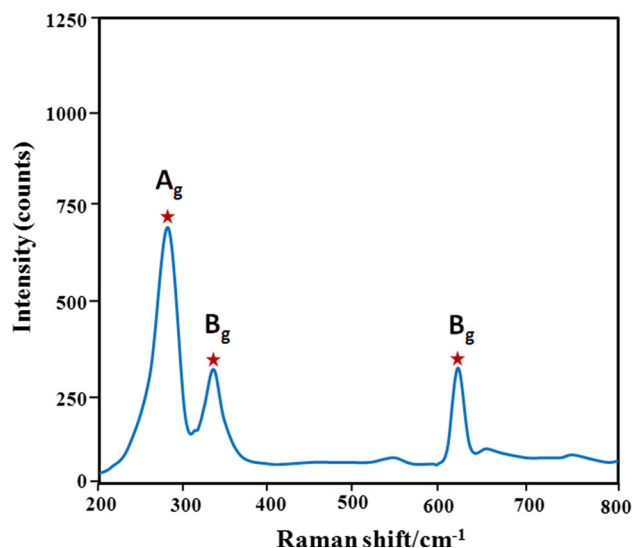


Fig. 6. Raman spectra of CuO.

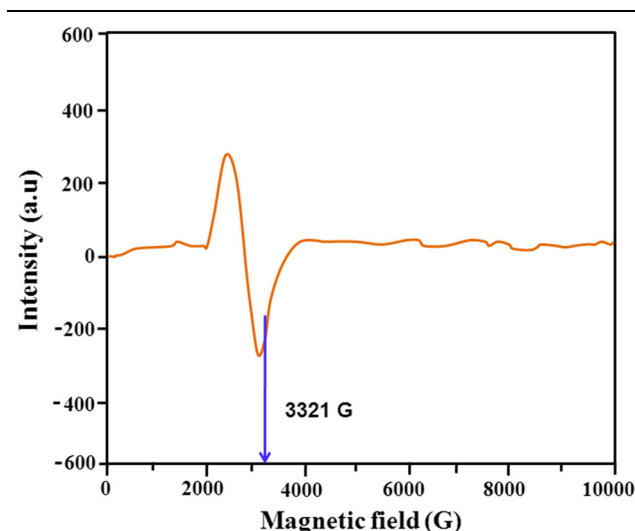


Fig. 8. Room temperature EPR spectra of CuO.

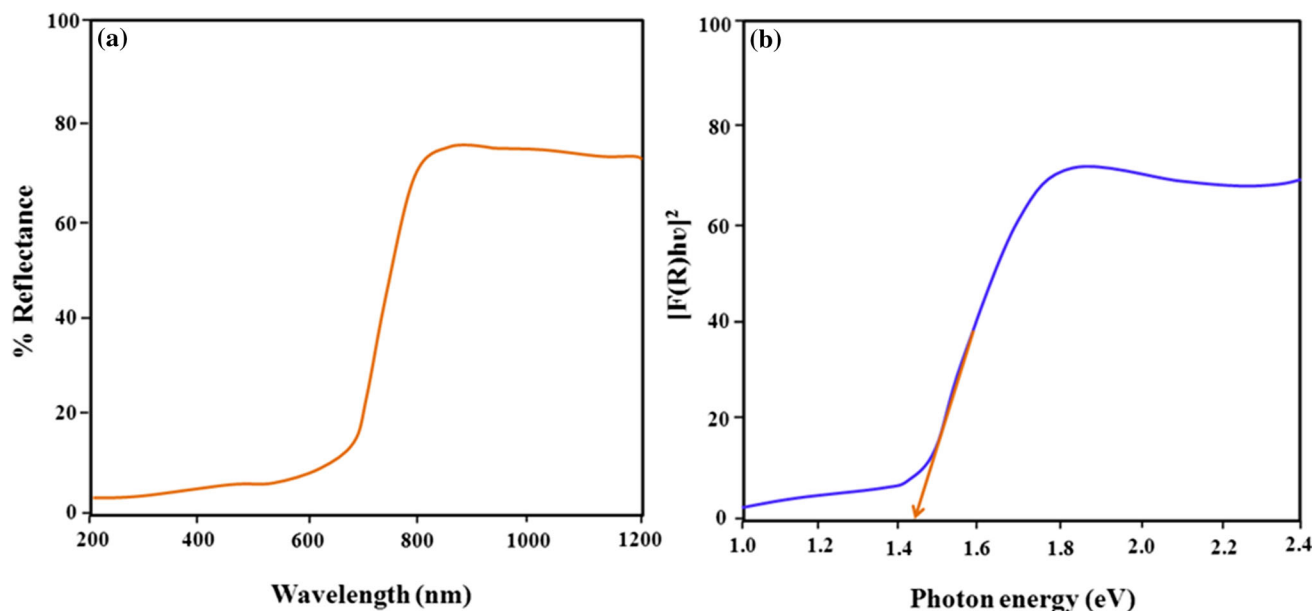


Fig. 7. (a) UV-Vis reflectance spectra of CuO and (b) band gap determination.

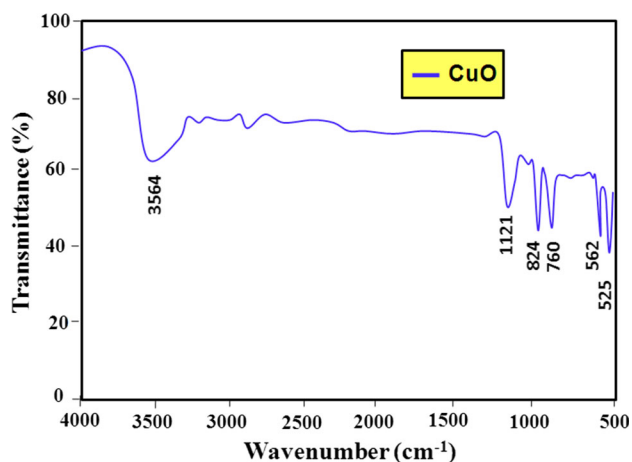


Fig. 9. FTIR spectra of CuO.

utilization of the active material. As a result, it induces the superior Faradic redox reactions and specific capacitance. At very high current density, the full surface utilization of a porous material is not possible and results in lower specific capacitance values. Figure 10d shows the charge–discharge assessment of the CuO electrode for 5000 continuous cycles under a high current density of 1 Ag^{-1} . The specific capacitance value decreases gradually with cycling, and an approximately 5.4% loss is observed after 2000 charge–discharge cycles at 1 Ag^{-1} .

Electrochemical Impedance Spectra (EIS) Analysis

EIS is an important tool to investigate the electrochemical characteristics of electrode/electrolyte interfaces using Nyquist plots, which

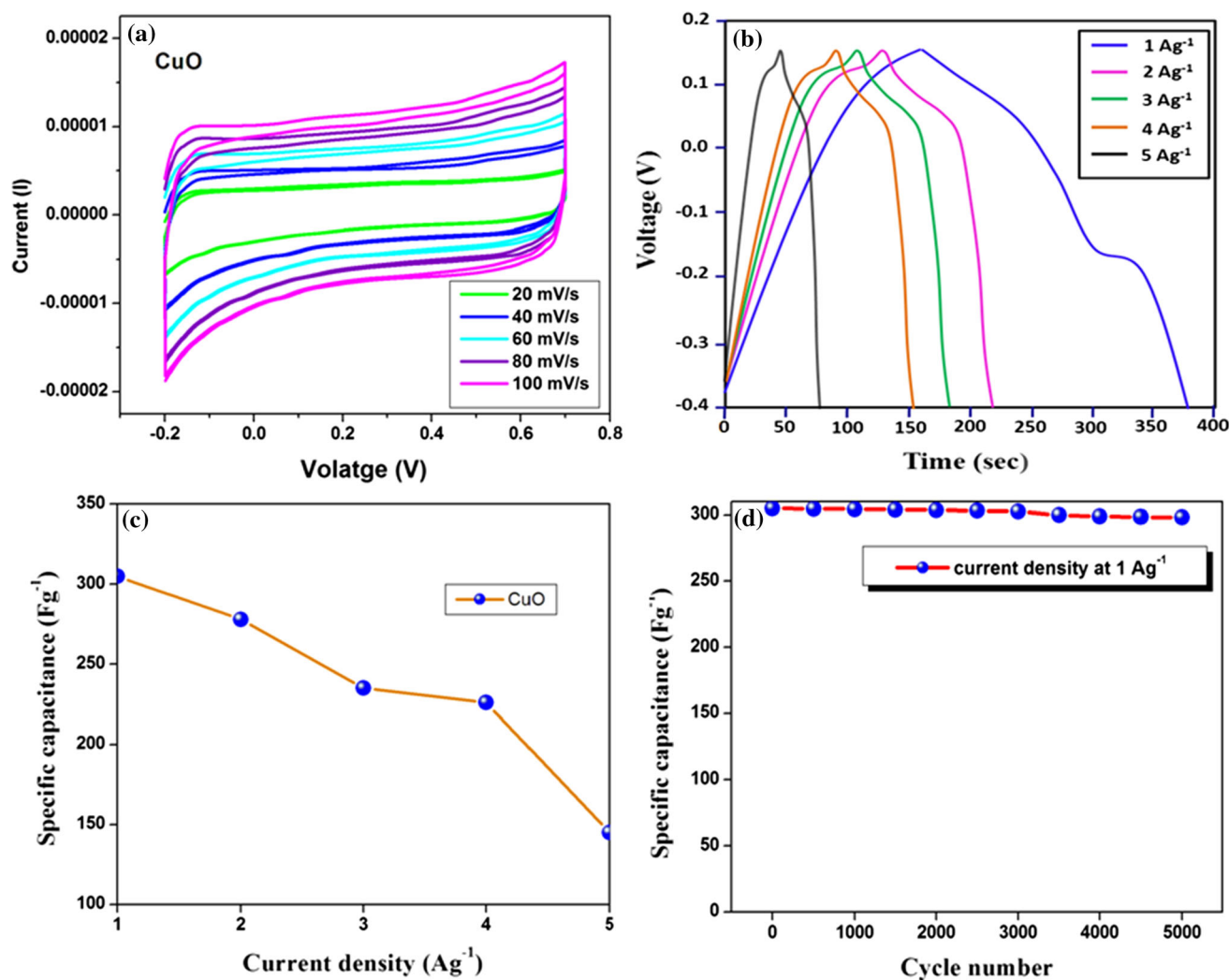


Fig. 10. (a) CV curves of CuO at different scan rates, (b) galvanostatic charging/discharging plots of CuO for various current densities, (c) variation in specific capacitance as a function of scan rate, and (d) cyclability test of the CuO electrode at a current density of 1 A g^{-1} .

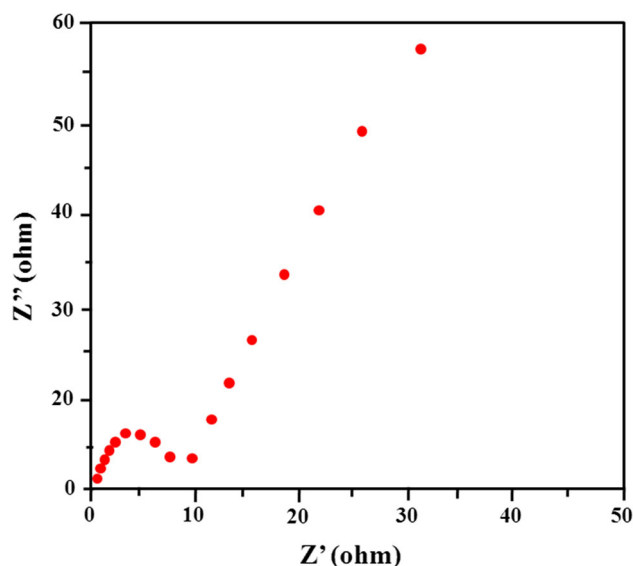


Fig. 11. Nyquist plots of the CuO electrode.

illustrate the real and imaginary parts of the EIS. The Nyquist plot of the CuO electrodes is shown in Fig. 11, from which it can be seen that a line is observed in the low-frequency region equivalent to the electron-transfer diffusion process. It is worth stating that, for perfect electrochemical capacitors, the Nyquist plot should be a line perpendicular to the real axis in the low-frequency region, although deviation from the ideal behavior is attributed to the pseudocapacitance properties of the oxide CuO rice like structure.

CONCLUSIONS

We have successfully prepared CuO with a nano-rice-like morphology by using a one-step hydrothermal method. It has the potential for fabrication at a large scale because the wet chemical route is facile and controllable. XRD and SEM results confirm that the CuO is single crystalline with a monoclinic structure and rice-like morphology. The XPS and EPR analyses also supported that Cu is in the 2+ state in CuO nanostructures. In the UV-visible absorption, a blue shift of band gap energy was observed with decreasing nanoparticle size due to the quantum confinement effect. The obtained CuO nano-rice-like electrodes exhibited a moderate specific capacitance and stable performance for supercapacitors. Considering the low

cost, abundant resources, the simplicity of the preparative method and the improved electrochemical properties, CuO nanostructures could be considered as promising electrode materials for electrochemical capacitors.

REFERENCES

1. P. Simon, Y. Gogotsi, and B. Dunn, *Science* 343, 1210 (2014).
2. G.P. Wang, L. Zhang, and J. Zhang, *Chem. Soc. Rev.* 41, 797 (2012).
3. M. Winter and R.J. Brodd, *Chem. Rev.* 104, 4245 (2004).
4. W.S. Seo, H.H. Jo, K. Lee, B. Kim, S.J. Oh, and J.T. Park, *Angew. Chem. Int. Ed.* 43, 1115 (2004).
5. V. Senthilkumar, F.B. Kadumudi, N.T. Ho, J.W. Kim, S. Park, J.S. Bae, W.M. Choi, S. Cho, and Y.S. Kim, *J. Power Sources* 303, 363 (2016).
6. X. Zhang, R. Gao, Z. Lia, Z. Hua, H. Liu, and X. Liu, *Electrochim. Acta* 201, 134 (2016).
7. J. Liu, N. Chen, and Q. Pan, *J. Power Sources* 299, 265 (2015).
8. Abhijit A. Yadav, T.B. Deshmukh, R.V. Deshmukh, and U.J. Chavan, *Thin Solid Films* 616, 351 (2016).
9. Y. Sun, L. Ma, B. Zhou, and P. Gao, *Int. J. Hydrogen Energy* 37, 2336 (2012).
10. L.J. Zhu, Y.T. Chen, Y.T. Zheng, N.X. Li, J.D. Zhao, and Y.G. Sun, *Mater. Lett.* 64, 976 (2010).
11. K.S. Jang and J.D. Kim, *Langmuir* 25, 6028 (2009).
12. Y.L. Liu, L. Lei, J.C. Li, and C.X. Pan, *J. Phys. Chem. C* 111, 5050 (2007).
13. X. Gou, G. Wang, J. Yang, J. Park, and D. Wexler, *J. Mater. Chem.* 18, 965 (2008).
14. A.L. Ortiz and L. Shaw, *Acta Mater.* 52, 2185 (2004).
15. M. Salavati-Niasari, N. Mir, and F. Davar, *Appl. Surf. Sci.* 256, 4003 (2010).
16. S. Layek and H.C. Verma, *J. Nanosci. Nanotechnol.* 13, 1848 (2013).
17. K. Karthik, N. Victor Jaya, M. Kanagaraj, and S. Arumugam, *Solid State Commun.* 151, 564 (2011).
18. M. Parthibavarman, K. Vallalperuman, S. Sathishkumar, M. Durairaj, and K. Thavamani, *J. Mater. Sci. Mater. Electron.* 25, 730 (2014).
19. R. Sasikala, K. Karthikeyan, D. Easwaramoorthy, I. Mohammed Bilal, and S. Kutti Rani, *Environ. Nanotechnol. Monit. Manag.* 6, 45 (2016).
20. W.Z. Wang, Q. Zhou, X.M. Fei, Y.B. He, P.C. Zhang, G.L. Zhang, L. Peng, and W.J. Xie, *Cryst. Eng Commun.* 12, 2232 (2010).
21. J.C. Irwin, J. Chrzanowski, T.D. Wei, J. Lockwood, and A. Wold, *Physica C* 166, 456 (1990).
22. W. Wang, L. Wang, H. Shi, and Y. Liang, *Cryst. Eng. Commun.* 14, 5914 (2012).
23. M. Parthibavarman, B. Renganathan, and D. Sastikumar, *Curr. Appl. Phys.* 13, 1537 (2013).
24. V. Hariharan, S. Radhakrishnan, M. Parthibavarman, R. Dhilipkumar, and C. Sekar, *Talanta* 85, 2166 (2011).
25. H. Siddiqui, M.S. Qureshi, and F.Z. Haque, *Optik.* 127, 3713 (2016).
26. M.M. Momeni, Z. Nazari, A. Kazempour, M. Hakimiyani, and S.M. Irhoseini, *Surf. Eng.* 30, 775 (2014).
27. L. Chen, L. Li, and G. Li, *J. Alloys Compd.* 464, 532 (2008).